



## Characterization of a microscale thermal–electrical field-flow fractionation system

Himanshu J. Sant\*, Bruce K. Gale<sup>1</sup>

State of Utah Center of Excellence for Biomedical Microfluidics, Departments of Bioengineering and Mechanical Engineering, University of Utah, 50 S. Central Campus Drive, Rm. 2110, Salt Lake City, UT 84112, USA

### ARTICLE INFO

#### Article history:

Received 4 October 2011

Received in revised form

18 December 2011

Accepted 19 December 2011

Available online 26 December 2011

#### Keywords:

Separation

Field-flow fractionation

Chromatography

Microfluidics

Nanoparticles

### ABSTRACT

A microscale thermal–electrical field-flow fractionation (ThElFFF) channel is reported for the first time and preliminary characterization results show high retention at certain operating conditions including relatively high flow rates when compared to standard microscale electrical or thermal field-flow fractionation instruments. A new design is presented that simplifies manufacturing and assembly of the prototype and that can provide both an electrical field and a high temperature gradient ( $\sim 10^6$  °C/m). Monodisperse particle retention is carried out with polystyrene nanoparticle samples to characterize the device. Retention ratios as low as 0.045 are observed with the ThElFFF instrument. Size selectivity of 1.77 was achieved for ThElFFF. The comparison with theory shows a marked deviation from the existing theory. Separation of a mixture of polystyrene particles is demonstrated for the first time using a ThElFFF system by separating 130 nm carboxylated polystyrene and 209 nm polystyrene particles.

© 2011 Elsevier B.V. All rights reserved.

### 1. Introduction

This paper presents the first multifunctional microscale field-flow fractionation system that is capable of employing both electrical and thermal fields simultaneously. The first report on macroscale thermal–electrical field-flow fractionation was published in 1991 by Giddings [1] and consisted primarily of proof-of-concept experiments. This brief communication demonstrated retention of polystyrene particles in nonaqueous solutions and showed an increase in the retention of colloidal particles in the channel. Essentially no work was done on this technique until our group began working on it a few years ago [2]. Based on Giddings preliminary work, we hypothesized that if the operating conditions are tuned properly, the use of dual fields should increase the selectivity and improve the separation power of the instrument despite some of the inherent shortcomings of electrical field-flow fractionation (ElFFF) and thermal field-flow fractionation (ThFFF) separation systems. This work differs from Giddings' paper [1] in that we have used (i) an aqueous carrier (ii)

fabricated and characterized a microscale version of ThElFFF, and (iii) demonstrated separation results.

One of the main limitations of ElFFF is the low effective fields experienced in the channel due to the electrical double layer at the electrode and particle surfaces in aqueous environments [3,4]. Low effective fields (typically 1–3% of the applied field) have limited the applications of this technique over the years by limiting the retention power of the systems. One solution to this problem is the use of cyclical or alternating electrical fields [5–7], which produces much higher effective fields and can be tuned for specific separations, but can be used with only a limited range of carriers [8] and can be limited by low peak capacity (sample spreading at high retention) [6]. These limitations can be somewhat offset by using sample relaxation and a DC off-set voltage [9].

Similarly for thermal field-flow fractionation, the typical retention is found to be low with aqueous carriers. These reduced effective fields can limit the ability of these systems to independently separate small particles or low molecular weight compounds, since the fields produced may not be sufficient to overcome diffusion. If both electrical and thermal fields could be applied simultaneously, the range of particles that can be retained using microscale thermal and electrical systems might be extended. Hence, a dual system capable of applying both electrical and thermal fields would be an interesting development (Fig. 1).

Another important aspect associated with both thermal and electrical systems is that the separation efficiency improves with miniaturization. Miniaturization of these two FFF subtypes

\* Corresponding author. Tel.: +1 801 581 6549.

E-mail addresses: [himanshu.sant@utah.edu](mailto:himanshu.sant@utah.edu) (H.J. Sant), [gale@eng.utah.edu](mailto:gale@eng.utah.edu) (B.K. Gale).

URL: <http://www.mems.utah.edu> (B.K. Gale).

<sup>1</sup> Tel.: +1 801 792 7074.

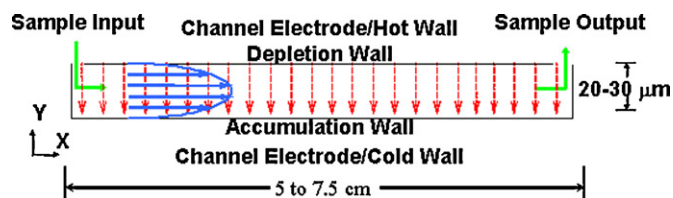


**Fig. 1.** Diagram of the operation of a FFF system showing the input and output ports, application of the field (thermal/electrical), the parabolic flow profile, and typical channel dimensions (not to scale). Electrical FFF requires channel electrodes at the depletion and accumulation walls, whereas thermal FFF employs a temperature gradient to induce the separation with the channel electrodes being replaced by hot and cold walls. It should be noted that “X” indicates the direction along the length of the channel and “Y” indicates the height direction of the channel.

provides increased resolution, faster analysis with lower power and reduced consumption of chemicals [10]. After the first report of a microfabricated electrical FFF (EIFFF) channel [11], a number of communications on other  $\mu$ -FFF subtypes including thermal [12], dielectrophoretic [13], flow [14], and cyclical electrical [15] have been reported in the last few years, indicative of increased interest in developing microscale field-flow fractionation instruments. Several ThFFF reports with excellent results were provided by Janča et al., in the last few years that utilized a mesoscale system with a channel thickness of 100  $\mu\text{m}$  and operating conditions that differ considerably from a system with a 25  $\mu\text{m}$  channel [16–18]. It should also be noted that the fabrication and assembly methods used by Janča et al. are the same as proposed by Giddings in the 1960s [19], except that the channel thickness was reduced to 100  $\mu\text{m}$  for most of the work. Only one paper has reported retention results in a 25  $\mu\text{m}$  thick ThFFF channel with relatively poor retention and without separation in a single run [20].

In this work, we propose a microscale-thermal electrical FFF system that is fabricated using rapid prototyping techniques [21]. This dual field system is expected to produce higher retention and resolution than existing single field FFF microsystems.

The challenges associated with an integrated FFF design for providing both electrical and thermal fields are numerous. The primary challenge is the choice and function of the channel walls due to the inherent presence of electrochemical effects associated with EIFFF in aqueous environments and the high heat fluxes needed for a miniature thermal system. The system also needs to provide efficient heat exchange to induce the required temperature gradient ( $\sim 10^6$   $^\circ\text{C}/\text{m}$ ) across the thin microchannel; otherwise a low temperature gradient and poor resolution result [13]. An efficient design of an integrated system requires heating/cooling of the EIFFF channel electrodes, most likely with an external cooling system. Typically a thermal FFF system is made with copper (for higher thermal conductivity) as the channel walls [22]. Even though this approach can yield a high temperature gradient, copper’s low electrochemical resistance makes it inappropriate for electrical FFF operation with aqueous carriers. The earliest microfabricated ThFFF system [12], with boron-doped silicon as the hot wall and glass as the cold wall, generated a poor temperature drop across the channel thickness. We have modified the basic design proposed in these reports by using silicon with high thermal conductivity as the cold wall and polished, very thin HDPE (high density polyethylene) with low thermal conductivity and high heat capacity as the hot wall. This arrangement was first communicated by us [2] and reported by others a short time later with glass as the hot wall [23]. A very thin hot wall ( $\sim 1$  mm) results in fast heating of the hot wall even with a low thermal conductivity high-density polyethylene (HDPE) wall. It should be noted that if proper insulation is not provided for a metal hot wall, considerable heat is lost to the ambient environment and a high energy input is required to maintain the steady and large temperature drop. In contrast the design modifications presented

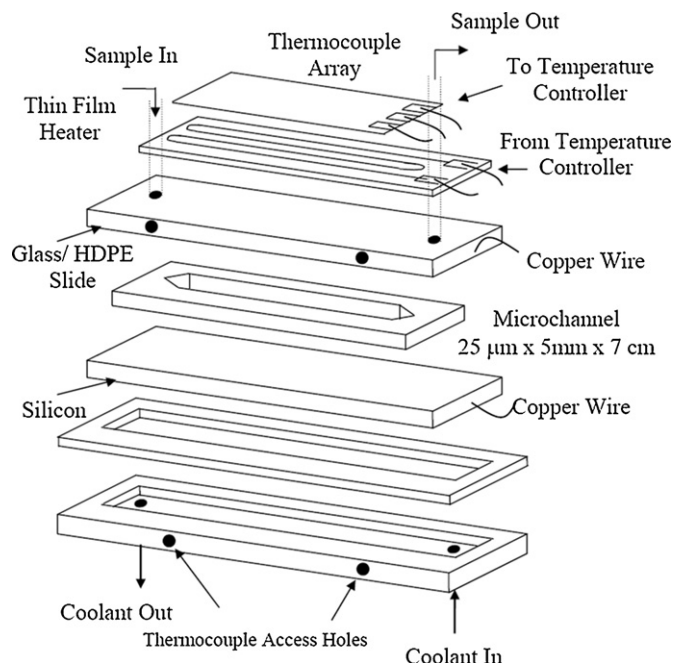


**Fig. 2.** Assembly diagram for the  $\mu$ -ThEIFFF device. The thermocouple array and heater consist of a thin film encapsulated in polyimide, and the microchannel is made from a 25  $\mu\text{m}$  thick double-sided adhesive tape. Copper wires in the figures will be used to connect the multimeter and power supply for the electrical field. Black circles on the sides of plastic slide indicate thermocouple holes for the thermocouple probes.

here result in a steady hot wall temperature and the high thermal conductivity of silicon allows for the fast removal of heat to maintain a low cold wall temperature. Fig. 2 shows a schematic of the various components of the micro thermal–electrical field flow fractionation ( $\mu$ -ThEIFFF) system prior to assembly.

## 2. Theory

### 2.1. Retention

General FFF retention theory is well developed and can be used to mathematically describe retention in the presence of simultaneous thermal and electrical fields. The retention ratio,  $R$ , is given by

$$R = \frac{t_0}{t_r} = \frac{V_0}{V_r}, \quad (1)$$

where  $t_0$  and  $V_0$  are the void time and volume, respectively and where  $t_r$  and  $V_r$  are the retention or elution time and volume, respectively.

Retention ratio is the basic parameter used to evaluate retention and can be related to the retention parameter as

$$R = 6\lambda \left[ \coth\left(\frac{1}{2\lambda}\right) - 2\lambda \right], \quad (2)$$

where  $\lambda$  is the retention parameter, a nondimensional number that relates the physiochemical property of the sample to the field. In its general form, retention ratio,  $R$ , and retention parameter,  $\lambda$  can be defined as

$$R = \frac{3d}{w} + \frac{6kT}{3\pi\eta d S_d U w}, \quad (3)$$

$$\lambda = \frac{kT}{Fw} = \frac{D}{Uw}, \quad (4)$$

and

$$F = \frac{kT}{\lambda w} = \frac{kTU}{D}, \quad (5)$$

where  $k$  is the Boltzmann constant,  $T$  is the temperature,  $w$  is the channel height,  $F$  is the force on the sample,  $D$  is the diffusion coefficient,  $U$  is the drift velocity of the sample in the direction of the applied field,  $S_d$  is the size selectivity, and  $w$  is the thickness of the microchannel. The drift velocity, which includes the effect of the applied field, is the particle velocity in the  $Y$ -direction due to the interaction of the external field (see Fig. 1). The drift velocities for electrical ( $U_E$ ) and thermal FFF ( $U_T$ ) systems are [24]

$$U_E = \mu E, \quad (6)$$

and

$$U_T = D_T \frac{\Delta T}{w}, \quad (7)$$

where  $\mu$  is the electrophoretic mobility of the particles,  $E$  is the effective electric field,  $D_T$  is the thermal diffusion coefficient, and  $\Delta T$  is the temperature gradient. The electrophoretic mobility can be given by Henry's law as

$$\mu = \left( \frac{2\varepsilon kT}{3\eta e} \right) f(\kappa a), \quad (8)$$

where  $\varepsilon$  is the dielectric permittivity of the medium,  $\kappa^{-1}$  is the Debye length,  $a$  is the particle radius,  $\eta$  is the carrier viscosity,  $e$  is the charge of the electron and  $k$  is the Boltzmann constant.

Force on the sample is additive in nature and can be related to the retention parameters for electrical and thermal system as

$$\frac{1}{R} = \frac{t_r}{t_0} = \frac{F_{TE}w}{6kT} = \frac{(F_T + F_E)w}{6kT}, \quad (9)$$

where  $F_T$  and  $F_E$  correspond to the thermophoretic and electrophoretic forces on the sample in the presence of the thermal and electrical fields.  $F_{TE}$  corresponds to the combined thermophoretic and electrophoretic forces and is given by [1]

$$F_{TE} = F_T + F_E, \quad (10)$$

From Eq. (5)

$$\frac{kT}{\lambda_{TE}w} = \frac{kT}{\lambda_T w} + \frac{kT}{\lambda_E w}, \quad (11)$$

where  $\lambda_{TE}$ ,  $\lambda_T$  and  $\lambda_E$  are the non-dimensional retention parameters for thermal–electrical, thermal, and electrical FFF respectively. On simplifying Eq. (11), we can obtain a relation for the collective  $\lambda_{TE}$  for the thermal–electrical system as

$$\lambda_{TE} = \left[ \frac{\lambda_T \lambda_E}{\lambda_T + \lambda_E} \right], \quad (12)$$

The steric-transition point in FFF is a strong function of the field strength and can be obtained by differentiating  $R$  (Eq. (3)) with respect to  $d$  and equating the result to zero and is given by

$$d_i = \left( \frac{2S_d kT}{3\pi\eta U} \right)^{1/(S_d+1)}, \quad (13)$$

where  $d_i$  is the steric-inversion diameter [3].

### 3. Experimental materials and methods

#### 3.1. Materials

##### 3.1.1. Samples

Polystyrene nanoparticles were purchased from Bangs Laboratories (Fishers, IN). Polystyrene particles with carboxylic groups on the surface typically have good retention in aqueous carriers in ThFFF [24]. Polystyrene nanoparticles have high UV

absorbance (~225 to 254 nm) and can easily be detected using an UV absorbance detector. These nanoparticles were diluted with DI water to 1% concentration by weight from the original sample to avoid detector saturation and overloading of the separation channel. Mainly three different types of particles: 91 nm, 130 nm (with a carboxylic surface group) and 209 nm polystyrene were used. The electrophoretic mobility of these samples ranged between  $2.0 \times 10^{-4}$  and  $4.0 \times 10^{-4}$   $\text{cm}^2 \text{V}^{-1} \text{s}^{-1}$  as measured using a zeta-potential analyzer (Zeta Plus, Brookhaven Instruments Corporation, NY). Sample injection volume for all experiments was 0.2  $\mu\text{L}$ .

##### 3.1.2. Carrier

Filtered DI water (Model D 8611, Barnstead International, IA) of  $18.2 \text{ M}\Omega\text{-cm}$  was used as the carrier for all the experiments. A 3  $\text{cm}^3$  gastight glass syringe (Model 1005, Hamilton CO., NV) was used to deliver fresh carrier fluid for each run.

##### 3.1.3. Electrode material

The original macroscale ThEFFF reported by Giddings was made with copper channel walls [1]. Copper, having a low electrochemical potential, is susceptible to vigorous electrochemical etching and deposition processes, which produces short-circuiting of the EFFF system after only a few uses in an aqueous environment. On the other hand, our group has successfully used gold, platinum [12], and graphite [10] based electrodes to fabricate EFFF systems. Other groups have successfully used titanium [25]. While graphite was found to have reproducible performance over long periods of operation, its low thermal conductivity limits its use in this particular system. In addition gold and platinum are expensive and hence, titanium was the preferred electrode material for the prototypes. The resistance of titanium electrodes along the length of the channel was less than  $5 \Omega$ . The connecting wires to the electrodes were glued with electrically conductive epoxy according to the manufacturer's directions (4011, Epoxy Technology Inc., MA).

To ensure the utility of titanium as a wall material, sample recovery experiments using titanium sputtered on a plastic substrate were performed and compared to results using glass and graphite. The results for the titanium were similar to that for glass and graphite channel walls, so titanium was selected for all future experiments.

### 3.2. Methods

#### 3.2.1. Instrument fabrication and assembly

Fig. 2 shows the schematic of the various components of the micro thermal–electrical field-flow fractionation system prior to packaging or assembly. The microfluidic channel is cut using a knife plotter (Graphtec, CA) in a 0.0025 cm thick pressure sensitive tape (9019, 3M, MN) and was sandwiched between the two substrates used as channel walls [10]. The geometrical dimensions of the microchannel are 0.0025 cm thick, 8.0 cm length and 0.5 cm width. A polished high density polyethylene (HDPE) slide was used to fabricate the first channel wall and was machined to provide the input and output ports for sample injection and carrier liquid transport. HDPE is used rather than glass to simplify the fluidic connections (Upchurch Scientific, MA). A thin film of titanium (2000 Å) was sputter deposited on the polished side of the HDPE substrate to create one of the electrodes for the EFFF part of the system. An identical titanium deposition was performed on the second or opposite channel wall, a silicon slide cut from a 100 mm diameter and 700  $\mu\text{m}$  thick silicon wafer.

All the thermal components (thin film heater, temperature sensor, controller (Minco, MN)) and cooler (Model 900, Fisher Scientific, PA) were external, as a part of our goal to realize simple, robust and inexpensive prototypes. A thin film heater with a thermocouple array was glued to the backside of the plastic slide with a

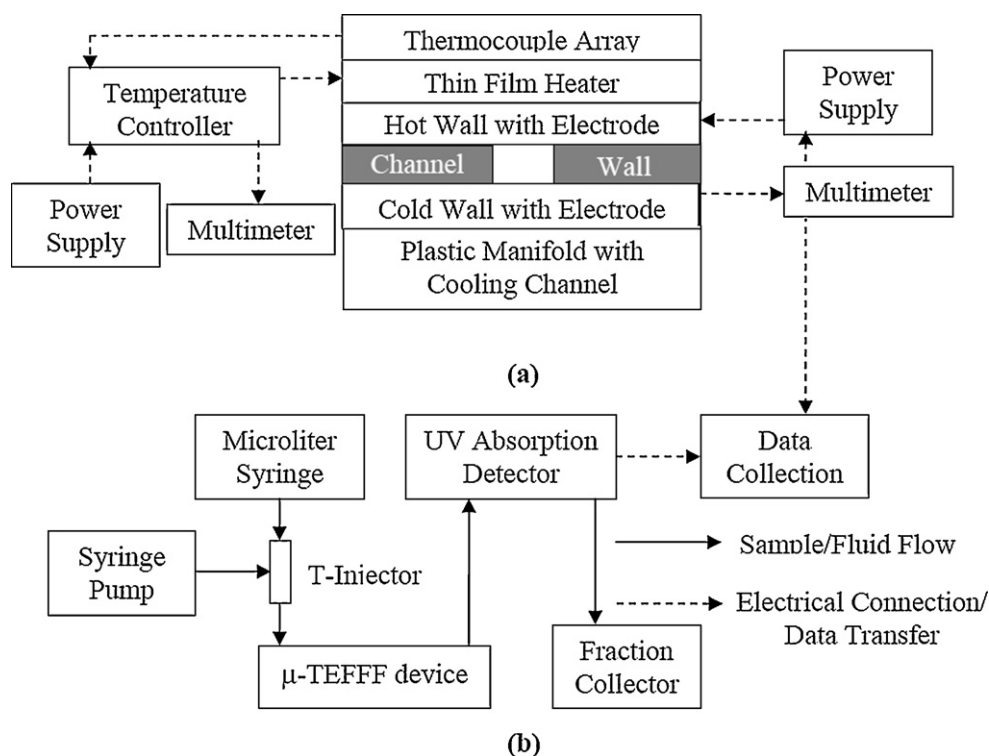


**Fig. 3.** Schematic of the experimental setup for  $\mu$ -ThElFFF system characterization. (a) The diagram shows the connections to the microsystem. (b) A diagram showing the instrumental experimental setup and the fluidic connection path.

deep groove to create a thin *hot wall* (1 mm thick). A set of thermocouple probes were connected to the holes drilled in the sides of plastic substrate for accurate temperature measurement. A temperature controller with feedback from the thermocouple array was used to control the thin film heater for the ThFFF part of the instrument. Similarly, holes were drilled in the heat exchanger on the *cold wall* side to access the silicon from the backside for the thermocouple probe. The difference in the temperatures of the hot wall and the cold wall was used as the overall temperature drop across the microsystem. It should be noted that the thermocouple arrangement and the digital thermometer (HH502, Omega Engineering Inc., Stamford, CT) used for the temperature measurement have  $\pm 2^\circ\text{C}$  accuracy.

### 3.2.2. Packaging and experimental setup

As shown in Fig. 3, a syringe pump (Model 220, KD Scientific Inc., MA) was used to deliver a constant flow of carrier fluid to the microsystem. The sample particles were injected using a microliter syringe (Model 701, Hamilton CO., NV) to the input port of the microchannel. All the fluidic connectors were purchased from Upchurch Scientific (Upchurch Scientific, MA). The T-injector facilitated the simultaneous transport of the carrier fluid and nanoparticle sample, while also preventing the unwanted dispersion of the sample in the carrier stream by avoiding mixing before entering the microchannel. The carrier fluid and sample particles passed through the ThElFFF channel and eluted to a  $9\ \mu\text{L}$  flowcell ( $1.2\ \mu\text{L}$  detector flowcell for separations in Fig. 10) of a UV absorbance detector (Model 520, ESA Inc, MA) through PTFE tubing 4 cm long with 0.076 cm inner diameter. The elution time/retention time of the sample was measured by the first moment of the elution peak recorded electronically using data acquisition hardware (DAQ card, model PC 6023 E, National Instruments, Inc. TX) and the interface software (Lab VIEW 6.1, National Instruments, Inc. TX). DC power supplies (Agilent E 3642 A and Tektronix PS 280) were connected to the ElFFF and ThFFF parts of the instrument,

respectively. A multimeter (Agilent 34401A, Agilent, CA) was used to continuously monitor the current between the ElFFF electrodes. The temperature difference across the microchannel was also recorded as shown in the layout in Fig. 2.

### 3.2.3. Retention and separation

A microscale ThElFFF system has never been demonstrated. The ThElFFF system was characterized by conducting retention experiments using polystyrene nanoparticles (diameters ranging from 91 nm to 209 nm). The temperature drop for the thermal field ranged from  $20^\circ\text{C}$  to  $45^\circ\text{C}$ . The applied voltage for the electrical field ranged from 1.5 V to 4.5 V. The flow rate range for these experiments was 0.5–2.0 ml/h. The sample injection volume was  $0.2\ \mu\text{L}$ . The retention time is converted to retention volume by multiplying by the carrier flow rate after subtracting the time taken by the sample to reach from the microsystem through the post-column tubing to the detector flowcell.

The walls of the ThElFFF system consisted of a thin, sputtered, titanium film on a plastic substrate. As we wanted to ensure minimal sample loss compared to conventional glass or graphite as FFF substrates, we first observed the amplitude of the detector response for the same sample volume and operating conditions (e.g. sample particles and flow rate) for different channel wall materials (glass, graphite and titanium). We compared the results for the three wall materials to verify that there was not unexpected sample loss using titanium. In later experiments we monitored the elution of the samples from the channel to ensure that sample recovery remained above 80%.

Retention in the  $\mu$ -ThElFFF system was characterized by observing the elution times of monodisperse polystyrene particle samples. All the experiments were geared towards obtaining data on retention time as this information can be converted directly to retention ratio. This retention ratio value was used to gauge the performance of the  $\mu$ -ThElFFF system by comparing the experimental results with the theoretical predictions.

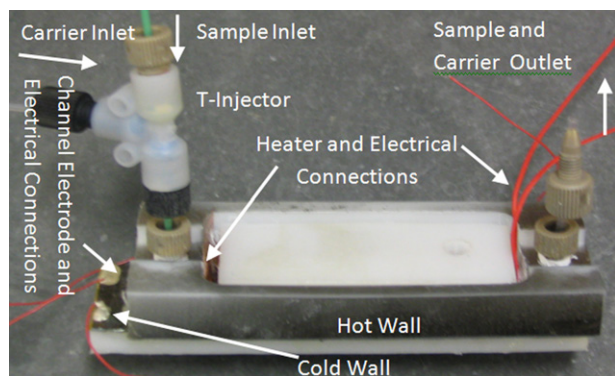


**Fig. 4.** A picture of a ThElFFF microsystem. The channel electrode and heater configuration along with fluidic connections are shown.

The main objectives of the characterization experiments were to (i) determine the optimal protocols and operational conditions and (ii) study the effect of important parameters that govern retention in a ThElFFF system. The most important parameters of interest are the temperature gradient and the electric field (voltage/channel width) across the channel. Other factors that may be important are flow rate, carrier composition, and sample size (particle diameter). This report characterized ThElFFF to determine only the effects of temperature gradient, voltage, flow rate and particle diameter.

Resolution is the main performance characteristic for any separation system and the  $\mu$ -ThElFFF was used to fractionate a nanoparticle sample mixture not resolved by individual  $\mu$ -ThFFF and  $\mu$ -ElFFF systems of 25  $\mu\text{m}$  channel thickness.

## 4. Results and discussion

### 4.1. Fabrication results

A photograph of the completed  $\mu$ -ThElFFF microsystem is shown in Fig. 4. Use of a plastic substrate with a conformal titanium layer as the hot wall was found to enable a robust approach for making fluidic connections by allowing the use of threaded fittings into the plastic substrate rather than ferrules glued to the microsystem (as used in previous microscale FFF systems) as shown in Fig. 4. There were no leaks during normal operation as reported with other systems [10]. It should be mentioned that the tape adhesion between the substrates became ineffective at very high temperatures ( $>85^\circ\text{C}$ ) and the system was replaced if any leakage occurred.

### 4.2. Voltage–current characteristics for ElFFF

The measured current across the ElFFF channel is a better indicator of effective field and the associated retention than the applied voltage [4]. This voltage–current relationship is different for every electrode material and carrier solution and must be characterized regularly. Titanium-based ElFFF systems typically require somewhat higher voltages than other ElFFF electrode materials for any current to flow due to the natural oxide layer that forms on the electrode surface.

The turn-on voltage for the titanium-based electrode system was measured to be about 3.7 V, which is much higher than that found for gold, platinum or graphite-based electrodes. We have not seen any bubbles associated with electrolysis that affect the retention over a long period of system usage.

The voltage–current relationship was also measured in the presence of a temperature gradient across the channel height, with no significant change in the relationship. This means that the effect of the temperature gradient on the *effective field* generated by the

**Table 1**

Representative elution data for the experimental runs in ThElFFF for 130 nm (carboxylated) particles and 1.5 ml/h flow rate.

Experiment	Electrical field		Temperature drop, $^\circ\text{C}$	Retention ratio
	Voltage, V	Current, $\mu\text{A}$		
1	3.5	25	30	0.0833
2	3.9	35	40	0.0454

ElFFF part of the system should not be significant. However, the particle electrophoretic mobility is a function of temperature (Eq. (7)) and it will be of interest to see whether temperature affects the electrical component of the retention in ThElFFF.

### 4.3. Sample recovery

Our experience with thermal FFF systems has shown that the sample recovery is lower for microsystems with plain glass or plastic channel walls when compared to the sample recovery in systems coated with a thin titanium layer. It was observed that particle adsorption progressively increases with time and system usage, especially under high fields. It should be noted that all of the experiments completed in this work do not use any detergents in the carrier solution, which is often helpful in increasing sample recovery. Future experiments may need to include a small fraction of detergent in the carrier solution to help to reduce sample adsorption on the channel walls.

### 4.4. ThElFFF retention behavior

A series of experiments at flow rates ranging from 0.5 to 1.5 ml/h were conducted with 209 nm polystyrene particles as the sample and it was found that retention of the sample particles increases in TEFFF mode. The dataset in Table 1 shows a significant improvement in retention with ThElFFF field. Applying electrical and thermal fields simultaneously results in increased retention as seen by peaks 6 and 7 in comparison to only electrical (peaks 2 and 3) or thermal (peaks 4 and 5) field application as shown in Fig. 5.

The required sample relaxation time for FFF scales with the square of the channel height (for thermal and electrical subtypes) and only a few seconds of relaxation should be required for microsystems [3]. Accordingly, all of the following experiments use a 15 s stop-flow to relax the sample. Another advantage of sample relaxation is improvement in the repeatability of the microsystem. Without any equilibration, the retention of the particles was found to be unpredictable, but a clearer trend in retention emerged when sample relaxation was employed.

#### 4.4.1. Retention comparison of different applied fields

The effectiveness of applying a combined thermal–electrical field over individual electrical and thermal fields is depicted in Fig. 6. It can be seen that the retention of nanoparticles is relatively low when ElFFF and ThFFF are operated independently. It should be noted that for the given operating conditions, ThFFF generates better retention (lower retention ratio) than is seen for ElFFF operating alone, and helps explain the limited interest that has been seen in ElFFF. Fig. 6 shows enhanced retention of nanoparticles using ThElFFF compared to nanoparticles experiencing only one field and similar operating conditions. Interestingly, the magnitude of the currents (in the ElFFF part of the operation) required to achieve a given retention actually decreases (i.e. retention produced per unit of current falls), thus much higher retentions can be achieved if ThElFFF is operated at even higher currents.

While the standard deviations in Fig. 6 are small, they are still non-trivial. The reasons behind the non-trivial standard deviations in Fig. 6 may be related to complex interactions between sample

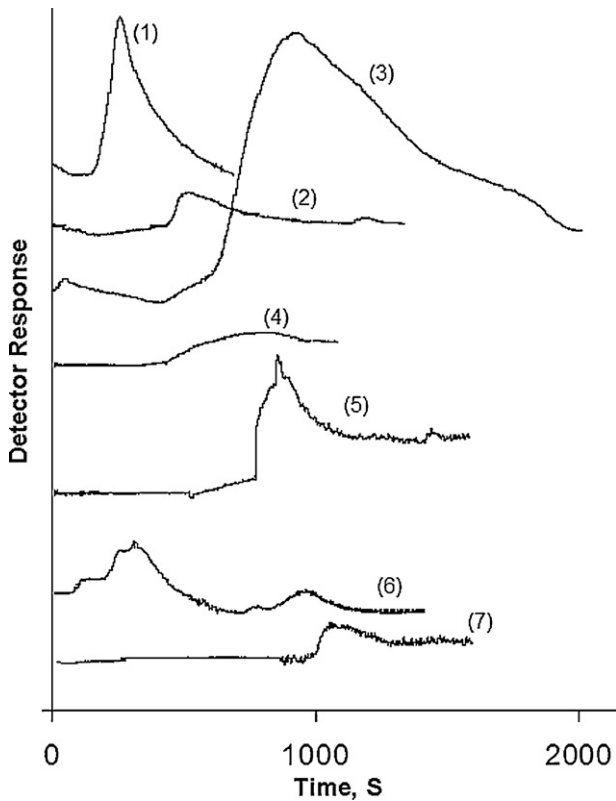


**Fig. 5.** Effect of applied electrical and thermal fields on retention for 209 nm diameter sample particles. Flow rate for each run was 0.8 ml/h. The applied field for fractograms is (1) no field, (2) 3.5 V, 30  $\mu$ A, (3) 3.6 V, 35  $\mu$ A, (4) 35  $^{\circ}$ C temperature difference, (5) 40  $^{\circ}$ C temperature difference, (6) 3 V, 20  $\mu$ A and 30  $^{\circ}$ C temperature difference, (7) 3.3 V, 30  $\mu$ A and 25  $^{\circ}$ C temperature difference.

properties (particle size, diffusion coefficients, electrophoretic mobility) and operational parameters (flow rate, flow profile, electrode condition, cooling wall condition, and uniformity of temperature across the system). For example if the resistivity of the DI water used changes from run to run, the effective field across the EIFFF system will change. A tighter control over operating conditions should result in more repeatable retention.

4.4.2. Retention with combined fields

Earlier we established that an increase in retention can be obtained for ThEIFFF in comparison with independent EIFFF or ThFFF operation, but a closer look at the retention behavior of ThEIFFF with a change in the combined fields is required to complete the characterization experiments.

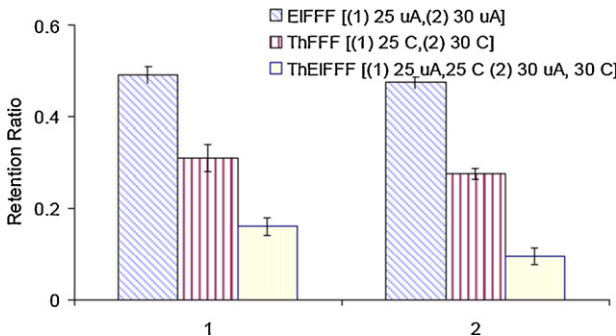


**Fig. 6.** Comparison of retention behavior of the different modes of FFF for 209 nm polystyrene particles.

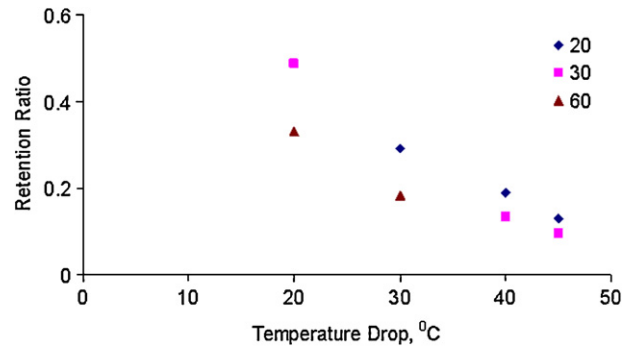


**Fig. 7.** Comparison of retention behavior with a change in the imposed temperature gradient and the applied electric field for 209 nm polystyrene particles. The x-axis shows the temperature drop in  $^{\circ}$ C for the thermal part of the combined ThEIFFF operation. The legend symbols indicate the current in  $\mu$ A for the EIFFF part of the combined ThEIFFF operation.

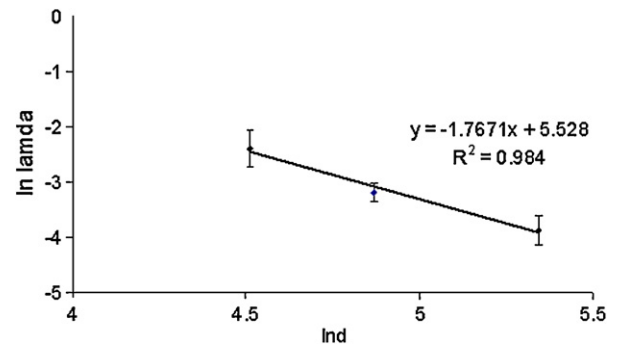


**Fig. 8.** The plot of retention dependence on size for ThEIFFF. The operating condition for this set of run are 30  $\mu$ A and 40  $^{\circ}$ C for the polystyrene particle sizes of 91 nm, 130 nm and 209 nm, respectively.

Retention data shown in Fig. 7 indicates that as the temperature gradient is increased for ThEIFFF, the amount of retention increases significantly even when small currents are applied as the EIFFF part of the operation. The additive nature of ThEIFFF results in enhanced retention with the use of electrical fields to augment the temperature gradient.

4.4.3. Size selectivity

Fig. 8 shows a linear relation between retention and particle size for ThEIFFF, which matches with conventional FFF theory. In addition, the measured slope of 1.77 in Fig. 8 is the size selectivity of

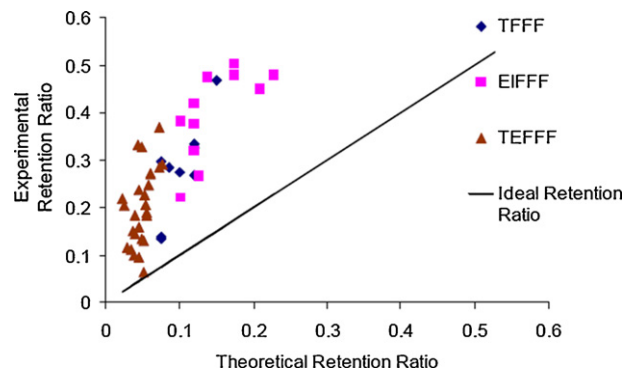


**Fig. 9.** Retention data for 209 nm particles at different operating conditions. Each data point for the theoretical retention ratio is calculated based on the corresponding operating conditions used for experimental runs and plotted against each other to show the deviation for the experimental data from the “Ideal Retention Ratio” line. Ideal Retention Ratio trace is a plot of theoretical retention ratio on both axes.

ThElFFF system. This measurement is slightly higher than that for thermal field-flow fractionation, which has size selectivity of about 1.5, and much higher than that for ElFFF, which has a predicted size selectivity of 1.0.

#### 4.4.4. Comparison with theory

Fig. 9 plots the measured retention ratio as a function of the theoretical retention ratio to see how closely the experiments compare to the theory. The line marked as “Ideal Retention Ratio” is a plot of theoretical retention ratio on both axes and would indicate a perfect match with theory. This straight line is used to compare the deviation of experimental data for a range of operating conditions (temperature gradient, voltage and flow rate).

It can be seen that both electrical and thermal FFF experimental results can show retention ratios as much as double the theoretical predictions. But it should be noted that for both electrical and thermal FFF a number of variables make it difficult to exactly predict the retention. For example, the effective field in ElFFF is not a straightforward ratio of applied voltage and channel height, but depends on factors such as ionic strength and pH of the carrier, surface charge on the particle in addition to not-so-well understood wall repulsion and particle–particle repulsion effects.

A partial explanation of the deviation from theory may involve the expected small steric transition point and secondary effects such as wall repulsion [26] that may be heightened with temperature. The steric transition point refers to the particle size at which the retention deviates from the normal mode and becomes solely dependent on the particle size itself. The calculated steric transition diameter (Eq. (10)) for ThElFFF for the operating conditions used in Fig. 6 is close to 275 nm. The wall repulsion effects would also compress the particle cloud thickness more than predicted using normal-mode retention theory could result in an even earlier steric transition. The wall repulsion effects are not very well understood and theory behind it is not well developed for microsystems, especially ThElFFF [26].

Similarly there is not a good model to predict thermal diffusion coefficient and hence, it is difficult to predict the retention ratio for thermal FFF. All of these factors likely contribute to the deviations observed in Fig. 9. Fig. 9, however, also shows that for some experimental data the deviation from theory is relatively small and that, overall, higher retention is generated using ThElFFF when compared to ThFFF or ElFFF alone. These results with an aqueous carrier indicate that the use of combined fields in a ThElFFF system would induce better resolution than that obtained using microscale thermal [12] or electrical [4] systems, and that the ThElFFF system could

potentially be used as a separation tool with better packaging (e.g. on-chip detector).

#### 4.5. Separation

Fig. 10 shows the separation of PS particles of 130 nm and 209 nm diameter with at 2.0 ml/h in ThElFFF mode. The separation is relatively rapid compared to results obtained using other microscale FFF systems [11,12]. It should be noted that the plate height or separation efficiency of the elution peak is a major performance characteristic that limits the resolution ability of the separation system. In this case, the separation runs with 9  $\mu$ L detector flow cells were not able to resolve this set of particles, so a 1.2  $\mu$ L volume detector flow cell was used instead with the injected sample volume reduced to 0.1  $\mu$ L. This reduction in the detector flow cell and sample volumes resulted in the reduction in instrumental plate height to allow a size-based separation with reasonable resolution. The fractograms titled “ElFFF” and “ThFFF” show no particle resolution with wide peaks. The fractogram titled “ThElFFF” in Fig. 10 shows the separation of PS 130 nm and 209 nm particles using ThElFFF. The peak for 209 nm shows significant broadening and “lagging” in the fractogram with unwanted short “peaks”. We believe that the use of off-chip detector and post column tubing resulted in increased dispersion and peculiar shape of 209 nm peak. The reduction in dispersion and hence, resolution could be further improved if the postcolumn tubing and external detector flow cell are replaced by an on-chip detector.

### 5. Concluding remarks

This report shows that the integrated  $\mu$ -ThElFFF system is able to provide both high temperature gradients (higher than any previously reported microscale ThFFF system) and act as a multi-functional tool with high effective fields.

A combination ThElFFF instrument requires a unique manufacturing approach and optimized operating conditions to enhance the retention of samples. Sample relaxation (stop-flow for 15 s) is found to improve the repeatability of the microsystem but overall repeatability is not very high and will require a tighter control over the carrier properties to enhance the performance of the system. For some conditions, ThElFFF can produce nearly twice the retention that can be generated by only ElFFF or ThFFF. Also, for the experiments performed in this work, the effect of the thermal field is more pronounced than the electrical field when ThElFFF is being operated in *additive* mode. The deviation of the experimental data from current theoretical models indicates the need of better models to predict effective field and thermal diffusion coefficients for electrical and thermal FFF systems in future for a wide range of operating conditions.

One of the potentially more appealing advantages of the demonstrated ThElFFF system is the increased range of size and type of the sample that can be analyzed with FFF microsystems. This microsystem also has the potential to contribute to not-so-well understood thermophoresis studies and electrophoretic analysis of samples of clinical and environmental interest. While operation of the thermal and electrical system in conjunction can increase the complexity of the retention mechanism, it can provide higher effective fields, lower plate heights and better resolution than can be obtained by stand-alone ThFFF or ElFFF systems of the same geometrical dimensions.

### References

- [1] G. Liu, J.C. Giddings, *Anal. Chem.* 63 (1991) 296.
- [2] H.J. Sant, B.K. Gale, 5th International Conference on Miniaturized Chemical and Biochemical Analysis Systems, Monterrey, California, October 21–25, 2001.

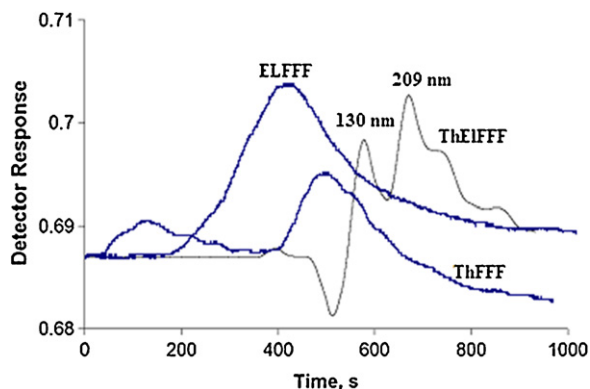


Fig. 10. Fractogram showing the binary separation of the polystyrene nanoparticle mixture using  $\mu$ -ThElFFF. The diameters of the particles being separated are 130 nm (carboxylated) and 209 nm. The separation is carried out in a single run with field of 3.6 V, 25  $\mu$ A and 30 °C temperature difference at a flow rate of 2.0 ml/h. The individual runs of ElFFF and ThFFF are operated at 25  $\mu$ A and 30 °C temperature difference at a flow rate of 2.0 ml/h.

- [3] B.K. Gale, K.D. Caldwell, A.B. Frazier, *Anal. Chem.* 73 (2001) 2345.
- [4] B.K. Gale, K.D. Caldwell, A.B. Frazier, *Anal. Chem.* 74 (2002) 1024.
- [5] B.K. Gale, S. Merugu, *Electrophoresis* 26 (2005) 1623.
- [6] A.I.K. Lao, D. Trau, I. Hsing, *Anal. Chem.* 74 (2002) 5364.
- [7] S. Merugu, H.J. Sant, B.K. Gale, *Electrophoresis* 31 (2010) 3372.
- [8] A.S. Kantak, S. Merugu, B.K. Gale, *Anal. Chem.* 78 (2006) 2557.
- [9] S. Merugu, B.K. Gale, 13th International Symposium on Field-and Flow-based Separation, Salt Lake City, Utah, June 27–30, 2007.
- [10] H.J. Sant, B.K. Gale, in: S. Hardt, F. Schönfeld (Eds.), *Microfluidic Technologies for Miniaturized Analysis Systems*, Springer-Verlag, Berlin, Germany, 2007, pp. 471–522.
- [11] B.K. Gale, K.D. Caldwell, A.B. Frazier, *IEEE Trans. Biomed. Eng.* 45 (1998) 1459.
- [12] T.E. Edwards, B.K. Gale, A.B. Frazier, *Anal. Chem.* 74 (2002) 1211.
- [13] T. Muller, T. Schnelle, G. Gradl, S. Shirley, G. Fuhr, *J. Liq. Chromatogr. Relat. Technol.* 23 (2000) 47.
- [14] D. Kang, M. Moon, *Anal. Chem.* 76 (2004) 3851.
- [15] A.S. Kantak, S. Merugu, B.K. Gale, *Lab Chip* 6 (2006) 645.
- [16] J. Janča, *Anal. Chim. Acta* 540 (2005) 187.
- [17] J. Janča, J. Stejskal, *J. Chromatogr. A* 1216 (2009) 9071.
- [18] J. Janča, V. Halabalova, J. Růžička, *J. Chromatogr. A* 1217 (2010) 8062.
- [19] G.H. Thompson, M.N. Myers, J.C. Giddings, *Anal. Chem.* 41 (1969) 1219.
- [20] J. Janča, *J. Chromatogr. A* 1046 (2004) 167.
- [21] H.J. Sant, B.K. Gale, *Sens. Actuators B* 141 (2009) 316.
- [22] M.E. Schimpf, in: M.E. Schimpf, K.D. Caldwell, J.C. Giddings (Eds.), *Field-Flow Fractionation Handbook*, Wiley-Interscience, New York, 2000, pp. 239–256.
- [23] S. Bargiel, A. Górecka-Drzazga, J.A. Dziuban, *Sens. Actuators A* 110 (2003) 328.
- [24] M. Schure, M.E. Schimpf, P. Schettler, in: M.E. Schimpf, K.D. Caldwell, J.C. Giddings (Eds.), *Field-Flow Fractionation Handbook*, Wiley-Interscience, New York, 2000, pp. 31–48.
- [25] R. Veen, K. Fromell, K.D. Caldwell, *J. Colloid Interface Sci.* 288 (2005) 124.
- [26] N. Tri, K.D. Caldwell, R. Beckett, *Anal. Chem.* 72 (2000) 1823.